STM JOURNALS

Research & Reviews: Journal of Physics
ISSN: 2278-2265 (Online), ISSN: 2347-9973 (Print)
Volume 8, Issue 1
www.stmjournals.com

The Effect of L-Valine on the Growth and Characterization of Lithium Sulphate Monohydrate Single Crystals

S. Bagavathi[1,*], C. Krishnan[2], P. Selvarajan[3]
[1]Scholar, Physics Research Centre, South Travancore Hindu College (affiliated to Manonmaniam Sundaranar University), Nagerkoil, Tamil Nadu, India
[2]Department of Physics, Arignar Anna College, Aralvaymoli, Tamil Nadu, India
[3]Department of Physics, Aditanar College of Arts and Science, Tiruchendur, Tamil Nadu, India

Abstract

Pure and amino acid doped good quality single crystals of Lithium Sulphate Monohydrate (LSM) were grown by slow evaporation solution growth technique at room temperature using water as solvent. The effect of amino acid (L-valine) dopant on the growth and characterization of LSM single crystal was investigated. Single-crystal X-ray diffractometer was utilized to find the unit cell parameters for pure and L-valine doped LSM crystals. The powder X-ray diffraction pattern of the grown crystals has been indexed. The modes of vibration of different molecular groups present in the samples were identified by the FTIR spectral analysis. The UV-vis-NIR studies were used to find the optical transmittance and the lower cut off wavelength. The mechanical properties of the grown crystals have been analyzed by Vickers micro hardness method. The thermal properties of both pure and L-valine doped LSM single crystals were studied by TGA/DTA measurements. The NLO property of L-valine doped and pure LSM crystals using KDP crystal as a reference were studied by SHG measurements.

Keywords: *Crystal growth, XRD, FT-IR, TGA/DTA, micro-hardness, NLO*

****Author for Correspondence*** E-mail: ms.bagavathi1972@gmail.com

INTRODUCTION

One of the most important current researches is nonlinear optics (NLO) because of its importance in emerging technologies such as frequency shifting, optical modulation and optical switching in telecommunications, signal processing, and optical interconnections [1]. Due to the lack of extended p-electron delocalization, the nonlinear inorganic materials have only the modest optical property, even though they are having good thermal and mechanical properties [2–5]. The growth, morphology and properties of the crystal can be modified by doping a small amount of impurity with pure material [6–9]. Amino acid crystals have good optical properties for developing telecommunications technologies [10–12]. Amino acids contain donor carboxyl acid (COOH) group and the proton acceptor amino (NH_2) group, known as zwitter ions which are more interesting materials for NLO applications. And above said groups create very strong hydrogen bonds, in the form of N–H+–O–C. Hydrogen bonds are used to generate non centro symmetric structure of NLO active materials [13–15]. In our present work, pure and L-valine doped Lithium Sulphate Monohydrate (LSM) single crystals have been grown and studied. The results of the growth, the single crystal X-ray diffraction studies, the powder X-ray diffraction studies, FTIR studies, UV-vis-NIR studies, micro hardness, TGA-DTA and SHG studies of the grown crystals are reported in this paper.

EXPERIMENTAL PROCEDURE

Crystal Growth

The commercially available Lithium Sulphate Monohydrate (AR grade) has been used to synthesize the LSM crystals. The starting material LSM ($Li_2SO_4.H_2O$) was taken and 20 g of material was dissolved in 70 ml deionized water at room temperature of 32°C. The calculated amount of 3 mol% L-valine (Merck-AR grade) was added with the pure

LSM saturated solution with constant stirring. The saturated solutions were prepared for pure and doped LSM separately and each was stirred well for 3 h to get homogenous solution. Repeated recrystallization was carried out in order to eliminate the impurities in the pure and doped LSM crystals and the solution was allowed to undergo slow evaporation which gradually led to supersaturated condition for the nucleation of crystal phase resulting in the formation of crystals. After a period of 35 days, good quality transparent single crystals of pure LSM with dimensions of 19 mm×11 mm×5 mm and L-valine doped crystals of LSM with dimensions of 11 mm×5 mm×4 mm were harvested successfully. The photographs of the grown crystal are shown in Figures 1 and 2.

RESULTS AND DISCUSSION

Single Crystal XRD Analysis

The X-ray diffraction studies for pure and doped crystals were carried out using Bruker Kappa Apex II diffractometer with Mercury Analyzer to determine the unit cell parameters. The observed lattice parameter values of pure and doped LSM crystals are tabulated in Table 1. It is observed that pure and doped LSM crystallize into monoclinic system and belong to $P2_1$ space group [16]. The observed results are good in agreement with the reported literature [17]. The XRD results confirm the incorporation of amino acid in the crystal lattice of LSM but do not change the crystal structure though there is a small change in the lattice parameters [18].

Powder XRD Analysis

Powder X-ray diffraction pattern of the grown crystals have been recorded using Bruker AXS D8 Advance (Cu, Wavelength 1.5406 A°) diffractometer. The pattern recorded for the undoped and L-valine doped LSM crystals scanned over the range of 10–80°.The recorded patterns are shown in Figures 3 and 4. The lattice parameter values of both pure and doped crystals, obtained from single crystal XRD studies, are confirmed by the powder XRD studies. The observed diffraction patterns are indexed and Miller indices are compared with the JCPDS database [19]. The XRD peak values of our present work are coincided with the reported values of the prominent peaks. Well-defined as well as intense peaks of XRD pattern at specific 2θ values indicate the high crystallinity of the pure and doped grown crystals and both the crystals are free from dislocations [20]. Some new peaks (0 2 1), (2 0 2), (2 2 2), (3 3 0), (111) and (1 1 2) were observed by doping of L-valine in pure LSM without changing the monoclinic structure of LSM. The peak intensities of reflections such as (0 0 1), (–1 0 1), (1 0 1), (0 2 2), (124) and (–1 2 5) were increased due to doping of amino acid [21].

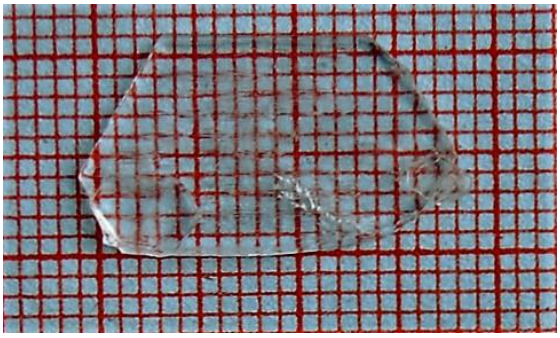

Fig. 1: *Photograph of Pure LSM.*

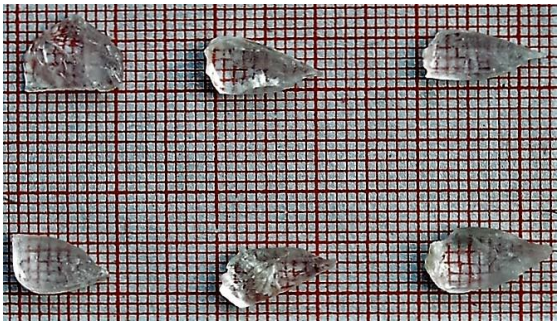

Fig. 2: *Photograph of L-Valine Doped LSM.*

Table 1: *Crystal Lattice Parameters of the Grown Crystals.*

Parameters	Single Crystal XRD (Pure LSM)	Single Crystal XRD (L-valine Doped LSM)	Reported [17] (Pure LSM)
a(Å)	5.452(2)	5.453(5)	5.4512(8)
b(Å)	4.853(2)	4.846(4)	4.8726(6)
c(Å)	8.161(3)	8.174(4)	8.1724(10)
α(°)	90	90	90
β(°)	107.30	107.26(3)	107.21(3)
γ(°)	90	90	90
Volume (Å^3)	207.26(2)	206.29(12)	207.26(5)
Crystal system	Monoclinic	Monoclinic	Monoclinic
Space group	$P2_1$	$P2_1$	$P2_1$

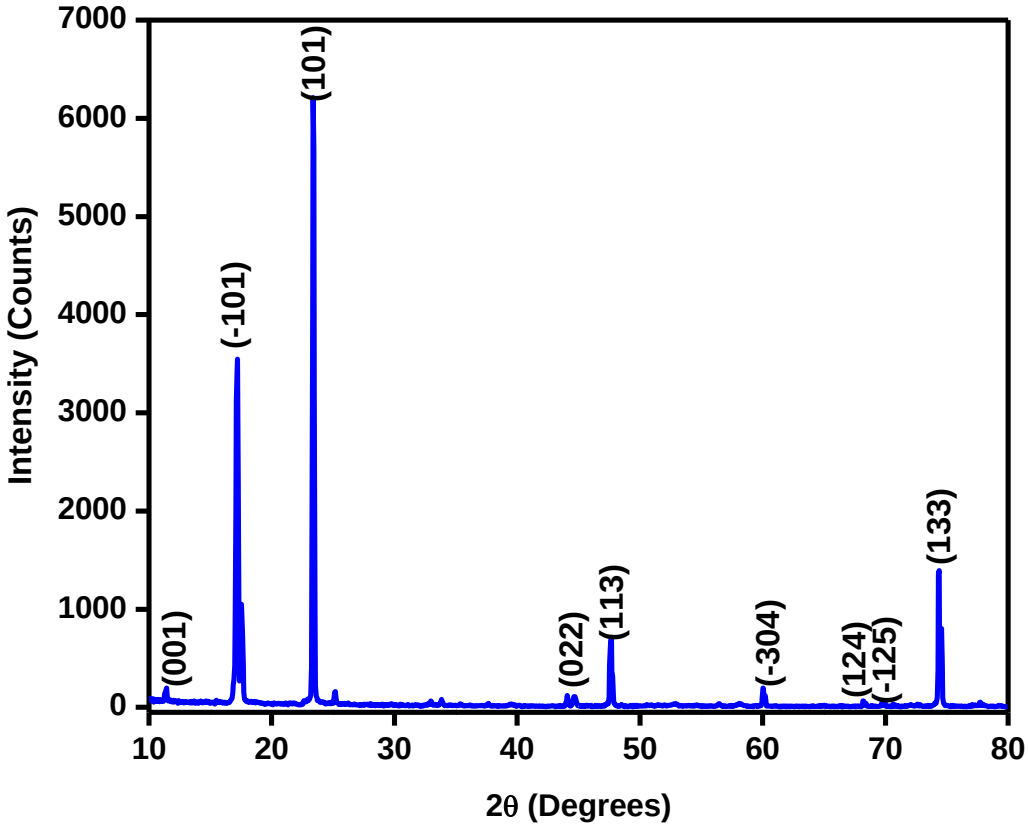

Fig. 3: *Powder XRD of Pure LSM Crystal.*

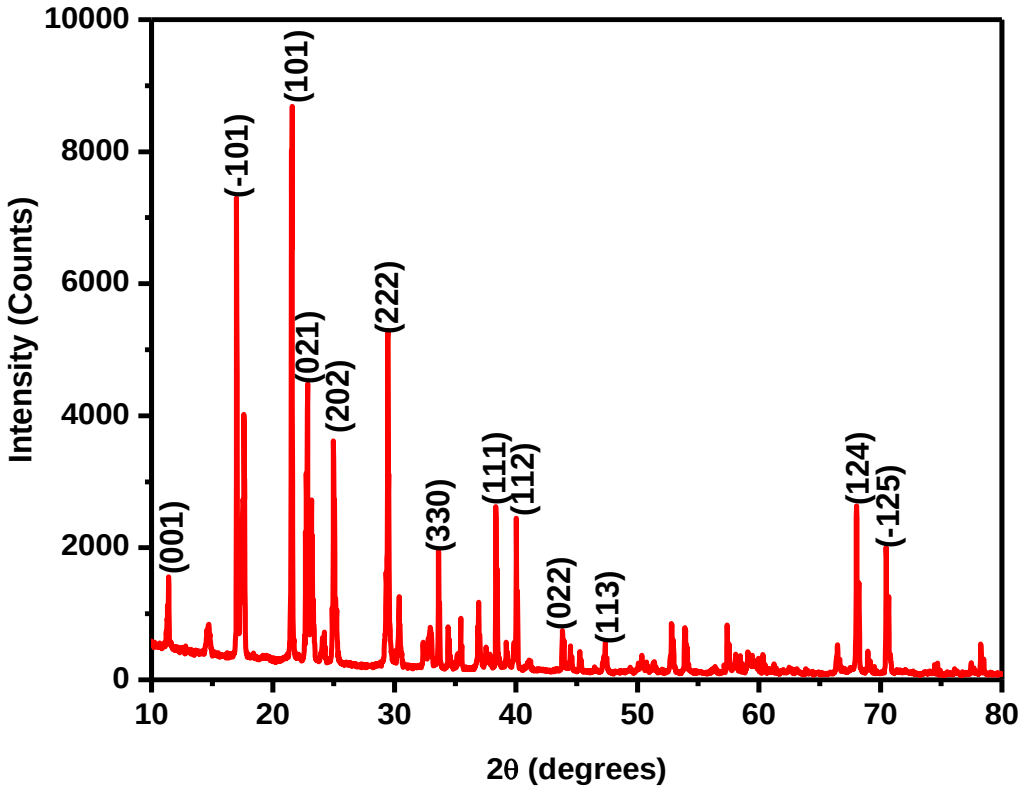

Fig. 4: *Powder XRD of Doped LSM Crystal.*

FT-IR Spectral Studies

The powdered samples of pure and L-valine doped LSM crystals were subjected to FT-IR analysis using Thermo Nexus 670 spectrometer with MCT-B Detector in the range 400–4000 cm^{-1}, which are shown in Figures 5 and 6. In this technique, almost all functional groups in a molecule absorb characteristically a definite range of frequency [22]. The shifts are observed in the peak positions of the spectra of doped crystals comparing with the spectra of pure crystals and hence the crystals are expected to have the interactions among the groups and ions. A broadband was observed around 3600–3300 cm^{-1} [23]. Symmetric stretching mode of O–H coordinated water molecule is observed around 3510.21 cm^{-1}. The medium broad band noticed around 1615.04 cm^{-1} is assigned to H–O–H bending of water molecules. The characteristic band observed at 2607.75 cm^{-1} (N-H…O valance stretching combination) and deformation bands (1606.83 and 1510.03 cm^{-1}) are due to the protonated amino group NH_3^+ [24]. The presence of broad band in high wave number region indicates the presence of hydrogen bonding in L-valine doped LSM crystals. This hydrogen bonding exists between carboxyl oxygen and amino nitrogen as reported by Dalhus and Gorbitz [25] Also, due to the zwitter ionic nature of amino acids, absorption bands occurred at 1403.37 cm^{-1} (COO-asymmetric stretching) and 1323.79 cm-1 (CO-stretching) [26]. Bands traced at 774.93 and 712.58 cm^{-1} are due to C-C skeletal and C-H out-of plane bending absorption bands with medium intensities supported their presence which are already reported [27]. The peak at 1110.48 cm^{-1} is attributed to SO_4 stretching mode (ν_3). A doubly degenerated vibrational mode (ν_2) and a triply degenerated vibrational mode (ν_4) are at 570.65 and around 641.20 cm^{-1} respectively. The mode at 482.04 cm^{-1} is assigned to the vibrational mode δ (Li-O). The above assignment agrees with the already reported values [28, 29]. The tentative assignments of the observed vibrational frequencies are listed in Table 2.

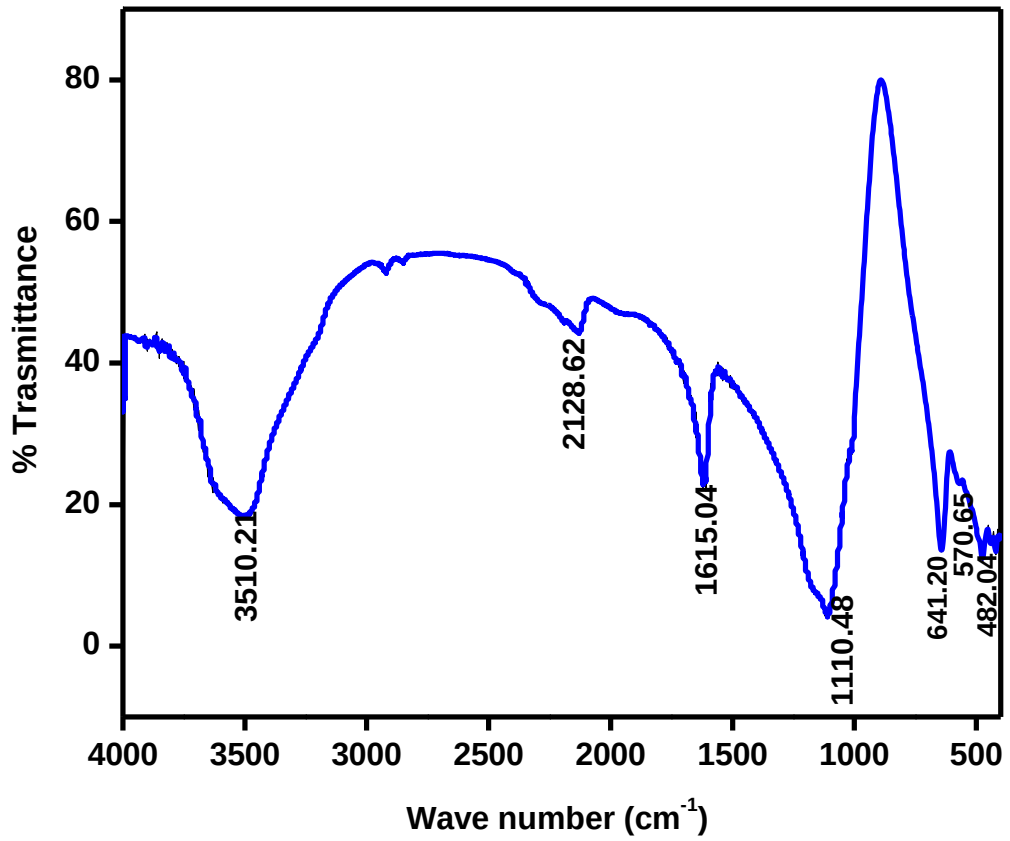

Fig. 5: *FTIR Spectral Data of Pure LSM Single Crystal.*

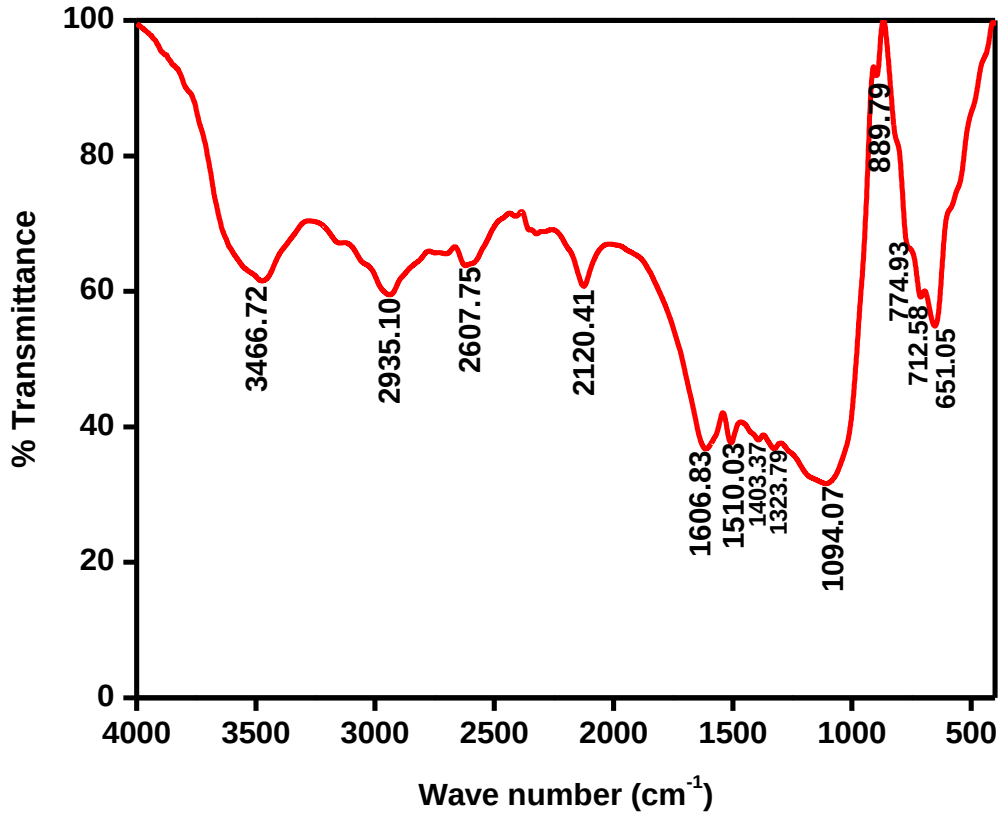

Fig. 6: *FTIR Spectral Data of Doped LSM Single Crystal.*

Table 2: *Functional Group Assignment of Pure and L-valine Doped LSM Single Crystals.*

Pure LSM Wave Number (cm^{-1})	L-valine Doped LSM Wave Number (cm^{-1})	Assignments
3510.21	3466.72	Symmetric stretching mode of the water molecule
2934.28	2935.10	CH_2 Symmetric stretching mode
--	2607.75	N-H…O valance stretching Combination
--	1606.83	NH_3^+ Asymmetric deformation
1615.04	--	Bending vibration of water molecules
--	1510.03	NH_3^+ Symmetric deformation
--	1403.37	COO- Symmetric stretching
--	1323.79	C-O Stretching
1110.48	1094.07	Stretching (ν_3) of SO_4
--	774.93	C-C skeletal Stretching
--	712.58	C-H out-of plane bending
641.20	651.05	Triply degenerate vibrations (ν_4) of SO_4
570.65	--	Doubly degenerate (ν_2) of SO_4^{2-} mode
482.04	--	Vibrational mode δ (Li-O)

Transmittance UV-VIS-NIR Analysis

Since single crystal is mainly used in optical applications, the optical transmission range and the transparency cut-off wavelength are essential. The UV-vis transmittance spectrum for pure LSM and L-valine doped LSM crystals is recorded using a UV-vis-NIR spectrometer in the range 190–800 nm**.** The recorded transmittance spectra are shown in Figures 7 and 8. Both pure and doped crystals show good transmittance in the visible region which enables them to be good optoelectronic materials. The percentage of transmittance decreases in doped crystals due to the growth of crystals at higher pH value (3.01) comparing with pure crystals [30]. The lower percentage of transmittance for doped crystals suggests that presence of L-valine enhances the optical activity of pure LSM crystal. The lower cut-off wavelengths for pure LSM and

L-valine doped LSM are found at 235 and 210 nm respectively. The lower cutoff wavelength of 210 nm of doped crystal is due the n–π^* transition of the carbonyl group of the carboxyl function and this transition will cause the near UV region absorption and nonlinear optical response. Using the transmittance T and thickness of the crystal d, we can calculate the absorption coefficient (α) of grown crystals by the relation, $\alpha = \frac{2.303}{d}\log\left(\frac{1}{T}\right)$. The grown crystals are obeying the relation between absorption coefficient and band gap energy, which is given as, $\alpha = \frac{A(h\nu - E_g)^{\frac{1}{2}}}{h\nu}$, where A is a constant. Using the Tauc's relation, Figures 9 and 10 have been plotted between ($h\nu$) and ($\alpha\ h\nu$)^2 for pure and doped crystals. The band gap (E_g) is determined by extrapolating the straight line portion of the curve to ($\alpha\ h\nu$)^2=0 [23]. From the plot, the band gap value of pure and L-valine doped LSM are found to be 5.44 and 5.92 eV respectively. The band gap values are calculated using the following formula, $E_g = \frac{1240}{\lambda}$ eV.

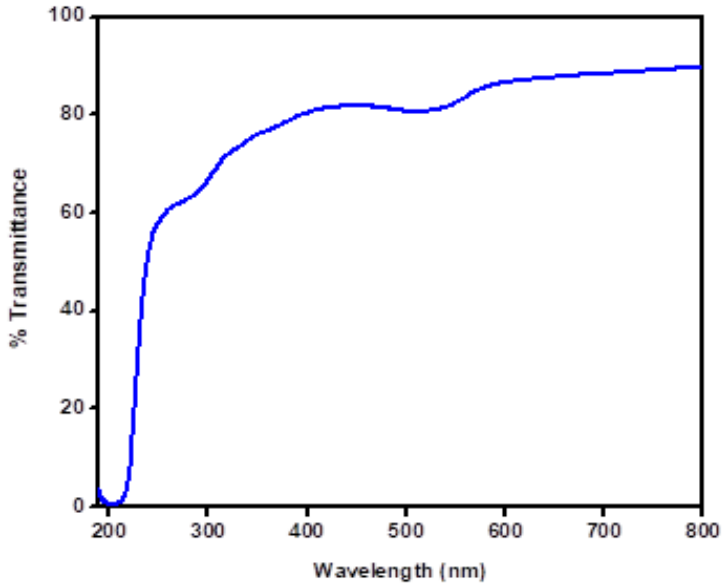

Fig. 7: *UV-Visible Transmittance Spectrum of Pure LSM Crystal.*

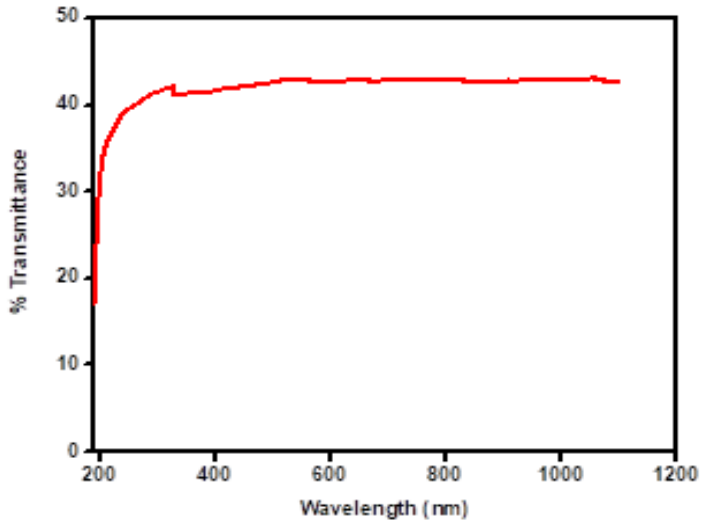

Fig. 8: *UV-Visible Transmittance Spectrum of Doped LSM Crystal.*

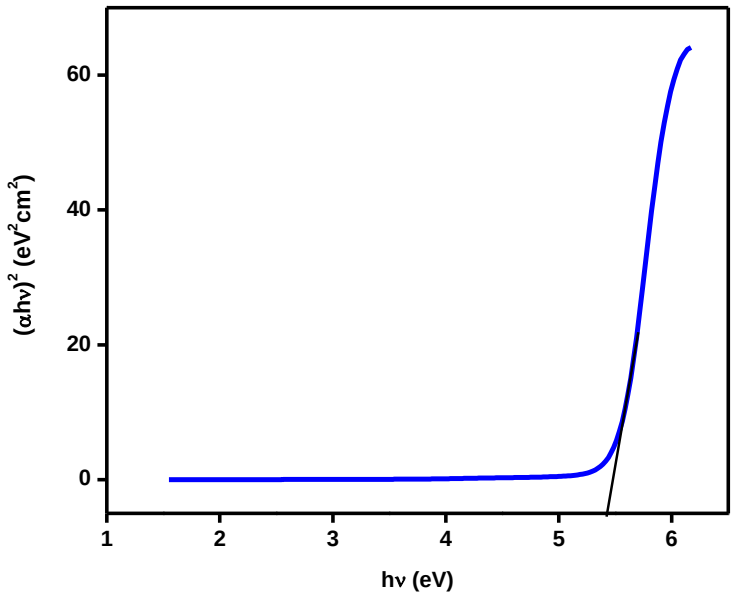

Fig. 9: *Tauc's Plot of Pure LSM Crystal.*

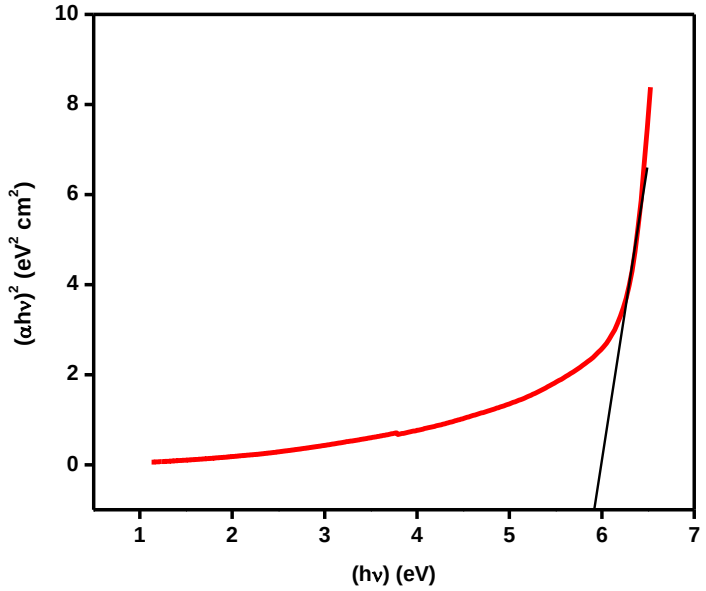

Fig. 10: *Tauc's Plot of Doped LSM Crystal.*

The calculated values are 5.28 and 5.91 eV respectively. The band gap values found by experiment have close agreement with calculated values. As the consequence of the wide band gaps of both the grown crystals, the crystals have large transmittance in the visible region [30, 31].

Mechanical Analysis

Microhardness testing of the grown crystals is one of the best methods to understand the mechanical properties of the materials such as fracture behavior, yield strength, brittleness index and temperature of cracking [32, 33]. The grown crystals of 4 mm thickness were well polished and placed on the platform of Vickers micro hardness tester. The indentations were made on (100) face of both pure and doped crystals. For the different loads varying from 25 to 100 g for the dwell time 5 s, the micro hardness measurements were made. The micro hardness values have been calculated by using the formula $H_v = \frac{1.8544 \times P}{d^2}$ kg/mm^2, Where, H_v is

the Vickers micro hardness number, P is the applied load in gram and d is in mm which is the average diagonal length of the indentation mark. When the load was increased from 25 to 100 gm, the hardness number was found to be increased. And above 100 g, the significant cracks and inclusions were observed, which may be due to the release of internal stress, generated locally by the indentation [34].

Figure 11 shows the variation of H_v as a function of applied load ranging from 25 to 100 g for pure and doped LSM single crystals. From the figures we can find that H_v increases with applied load. The doped and pure crystals have Vickers hardness number of 57 and 55 $kgmm^2$ for an applied load of 100 g respectively. Hardness number is slightly increased in doped crystals comparing with pure crystals. The hardness of the material is increased due to the doping of amino acid and hardness of the material depends on the concentration of the dopants. To find the value of 'n', a graph is plotted between log P and log d for pure and doped crystals (Figures 12 and 13). From the slope of the obtained straight line, we can find the value of work hardening coefficient 'n', whose value is 2.788 for pure LSM crystal, but for doped crystal, the value of n is 3.773. According to Onitsch and Hanneman, the n values are more than 1.6 for both pure and doped crystals and they are soft in nature [35]. From the obtained n values, we came to know that both the pure and doped crystal have high mechanical strength and they can be used for device applications. Due to the high 'n' value, the doped crystals are having more mechanical strength than pure crystals.

Thermal Analysis

Simultaneous thermogravimetric analysis (TGA) and differential thermal analysis (DTA) of pure and doped crystals were carried out using a STD Q600 V8.3 build 101 thermal analyzer. The TGA and DTA are carried out from the temperature 40 to 750°C at 20°C/min in the nitrogen atmosphere. The thermo gravimetric results are governed by the weight and particle size. In practice, a small sample weight is desirable for thermo gravimetric results and hence the weight of the sample taken for investigation is 13.159 mg [36]. TGA and DTA are plotted for pure and doped crystals (Figures 14 and 15). Below 150.4°C, there is no detectable weight loss which shows that there is no decomposition up to this point and this will be insured thermal stability of material for possible application in lasers. The sharp weight loss was observed at 156.35 and 150.4°C for pure and doped crystals respectively without any intermediate stages. We can observe the loss of one water molecule at the temperature of 156.35°C for pure LSM crystal and 150.4°C for doped LSM crystal. This is inferred from the exothermic peaks observed near 156 and 150°C in DTA for pure and doped crystals respectively. The decomposition temperature range observed is 95–745°C for pure and 98.6–740°C for doped crystals. The prominent endothermic peaks of DTA curve observed at 578.47 and 573.3°C represent the melting point of pure and doped crystals respectively. These values coincided with thermo gravimetric values, which confirmed the thermal stability of the crystal [37]. The 85.99 percentage weight of the sample remains after the water molecule is released for both doped and pure crystals, which matches well with the observed value of 86%. Hence, we came to know that the thermal stability of the pure crystal and doped crystal is very high. The L-valine doped crystals show the same features of pure LSM, but there is a small shift in the decomposition temperature.

NLO Study

The second harmonic generation property of NLO material is determined by the Kurtz and Perry powder technique [38]. The presence of delocalized π-electron systems, which will connect the donor and accepter groups, is the microscopic origin of non-linearity in the NLO materials. This will enhance the asymmetric polarizability of the material. Each type of constituent chemical bond, as a part, contributes to the total non-linearity of the whole crystal. The distribution of valence electrons of the metallic elements is an important factor that strongly affects the linear and nonlinear properties of each type of constituent chemical bond [39]. Second harmonic generation efficiency of pure and doped LSM is found with the help of 1064 nm wavelength of Nd:YAG laser beam. The SHG analysis of grown crystals is shown in

Figure 16. The laser beam is made to fall on the powdered samples of pure and doped crystals. From the emission of intense green radiation (λ=532 nm) by the sample, the second harmonic behaviour of the crystals is confirmed for both the samples. The SHG efficiency of pure LSM is found to be 1.32 times that of KDP crystal and it is 1.26 times that of KDP for doped LSM crystal. The reported value of second harmonic efficiency of pure L-valine is 0.82 times that of KDP [40]. Hence, when the L-valine is doped with LSM crystal, L-valine decreases the SHG efficiency of LSM. And also we can conclude that the decrement of SHG efficiency of the doped crystal is due to the disturbance of electronic charge distribution in the amino acid doped crystals [41].

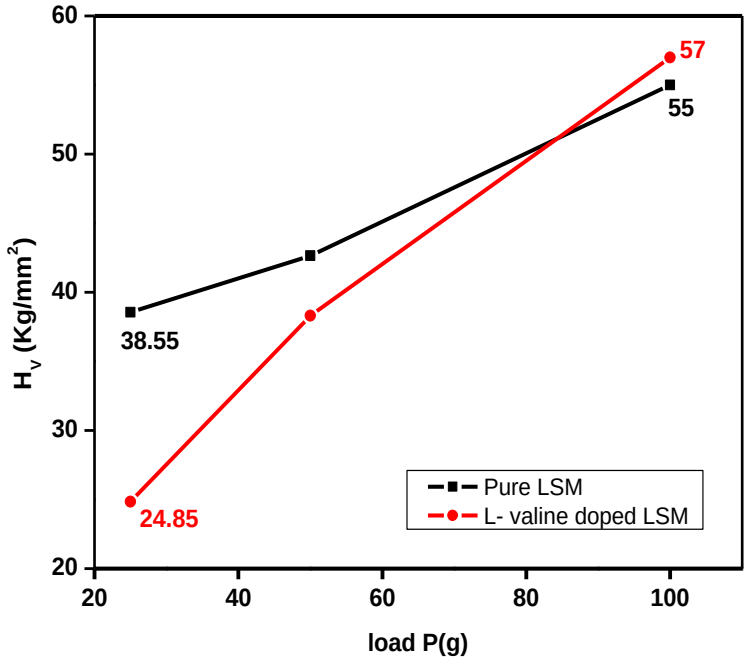

Fig. 11: *Variation of Micro Hardness with Load for Pure and Doped LSM Crystals.*

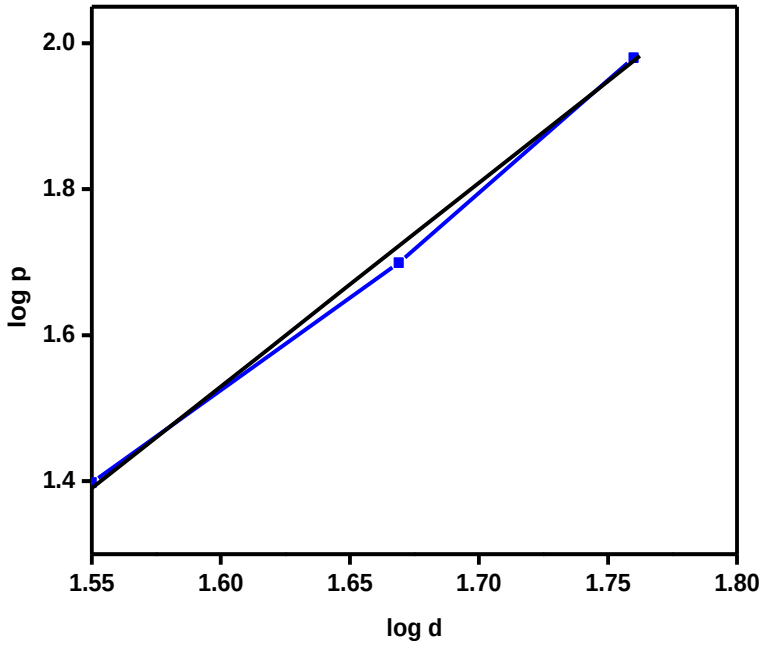

Fig. 12: *Graph between log P verses log d of Pure LSM Crystal.*

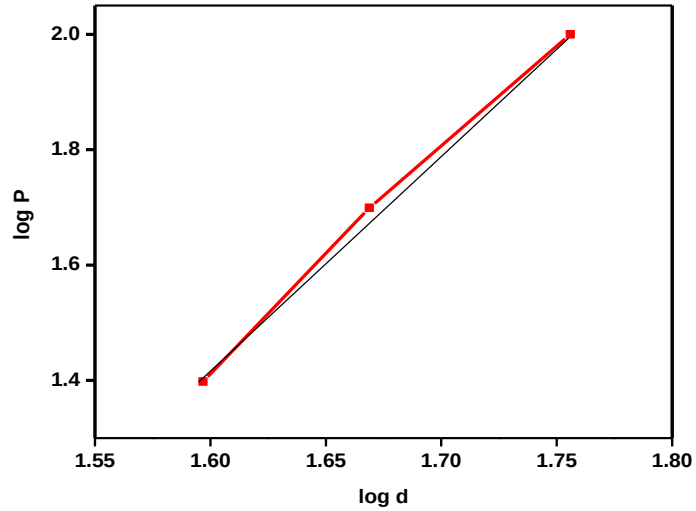

Fig. 13: *Graph between log P verses log d of Doped LSM Crystal.*

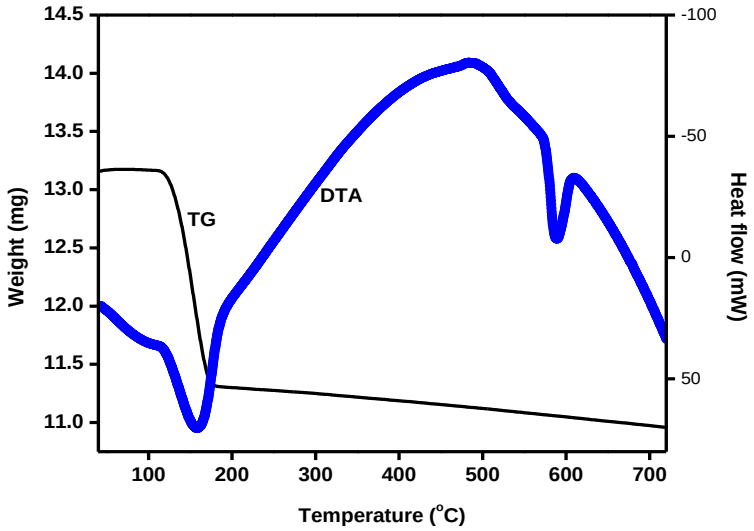

Fig. 14: *TG/DTA Curves for Pure LSM Crystal.*

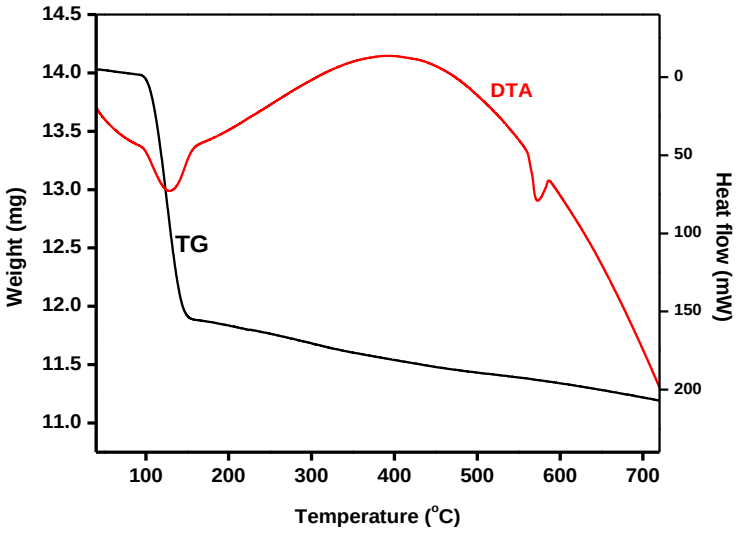

Fig. 15: *TG/DTA Curves for Doped LSM Crystal.*

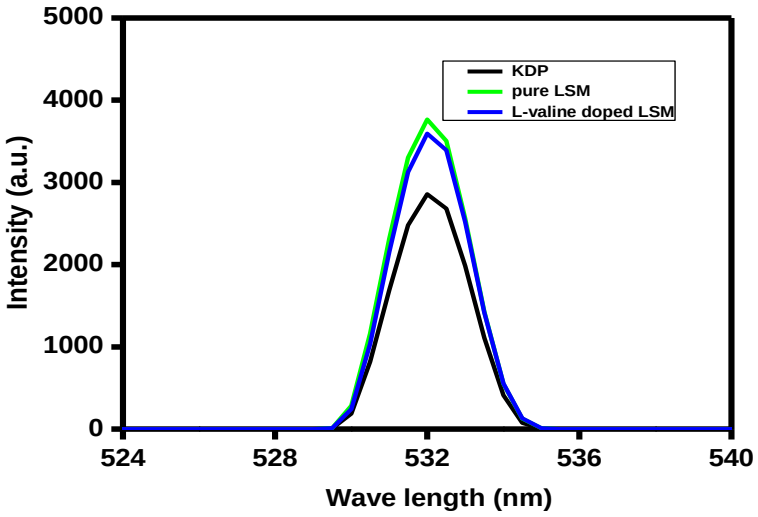

Fig. 16: *SHG Analysis for LSM and Doped LSM Crystals.*

CONCLUSION

Good quality pure and L-valine doped LSM crystals are grown using slow evaporation method. The grown crystals are characterized by using single crystal X-ray diffraction technique which confirms the monoclinic structure of both pure and L-valine doped single crystals with slight variations in the crystal lattice parameters. In powder crystal X-ray diffraction pattern, we observed the extra peaks in the doped crystals, which show the incorporation of amino acid with pure LSM. The functional groups present in the pure and doped crystals have been confirmed by FTIR spectral analysis. From UV-vis-NIR analysis, it is confirmed that both the pure and doped crystals are having wide range of transparency from 190–800 nm. Micro hardness analysis reveals that the hardness is less for doped crystals than pure crystals and both the doped and pure crystals belong to soft materials. From the thermal property, we came to know that both the pure and doped crystals are stable up to the temperatures 156.35 and 150.4°C respectively and we can observe that there is an increase of decomposition temperature in doped crystals, which confirms the stability of the grown crystals. The powder SHG test confirms that the NLO property of doped crystal is less than that of pure LSM crystal. But NLO property of both pure and doped crystals is more than that of KDP. Therefore it is concluded that the inorganic pure LSM and L-valine doped LSM are promising NLO materials with enhanced SHG efficiency.

ACKNOWLEDGEMENT

The author is grateful to the management of National Engineering College, Kovilpatti, for the encouragement given to carry out the research work. Research supports given by Aditanar College of Arts and Science, Tiruchendur, STIC, Cochin University, and St. Joseph's college, Trichy, IISC, Bangalore are gratefully acknowledged.

REFERENCES

1. Pal T, Kar T, Boceli G, *et al. Cryst Growth Des*. 2004; 4: 743–747p.
2. Mercy HO, Rosker MJ, Warren LF, *et al. Opt Lett*. 1995; 20: 252p.
3. Mohankumar R, Rajan Babu D, Ravi G, *et al. J Cryst Growth*. 2003; 250: 113–117p.
4. Ariponnammal S, Radhika S, Vennila RS, *et al. Cryst Res Technol*. 2005; 40: 786–788p.
5. Sun HQ, Yuan DR, Wang XQ, *et al. Cryst Res Technol*. 2005; 40: 882–886p.
6. Simon B, Boistelle R. *J Cryst Growth*. 1981; 52: 779–788p.
7. Clydesdale G, Roberts KJ, Docherty R. *J Cryst Growth*. 1994; 135: 331–340p.
8. Veintemillas-Verdaguer S. *Prog Cryst Growth Charact Mater*. 1996; 32; 75–109p.
9. Sangwal K, Mielniczek-Brzoska E. *J Cryst Growth*. 2002; 242: 421–434p.
10. Frazier CC, Cockerhamn MP, Chauchard EA, *et al. J Opt Soc Am B.* 1987; 4: 1899–1903p.
11. Monaco SB, Davis LE, Velsko SP, *et al. J Cryst Growth*. 1987; 85: 252p.

12. Gunter P, Bosshard Ch, Sutter K, *et al. Appl Phys Lett.* 1997; 50: 486p.
13. Yukawa Y, Inomata Y, Takeuchi T, *et al. Bull Chem Soc Jpn.* 1982; 55: 3135p.
14. Yukawa Y, Inomata Y, Takeuchi T. *Bull Chem Soc Jpn.* 1983; 56: 2125p.
15. Itoh S, Yukawa Y, Inomata Y, *et al. Bull Chem Soc Jpn*. 1987; 60: 899p.
16. Boopathi K, Ramasamy P, Bhagavannarayana G. *J Cryst Growth*. 2014; 386: 32–37p.
17. Selvapandiyan M, Arumugam J, Karthikeyan S, *et al. Journal of Environmental Science, Computer Science and Engineering & Technology (JECET)*. 2017; 6: 523–530p.
18. Benila BS, Bright KC, Mary Delphine S, *et al. J Magn Magn Mater*. 2017; 426: 390–395p.
19. Swanson Howard E, Marlene C, *et al.* Standard X-ray Diffraction Powder Patterns. *National Bureau of Standards Monograph*. 25-Section 4, Issued Jun 28, 1966.
20. Latha Mageshwari PS, Priya R, Krishnan S, *et al. Optik*. 2014; 1–6p.
21. Russel Raj K, Bhagavannarayana G, Murugakoothan P. *Optik*. 2013; 124: 493–500p.
22. Kalsi P. *Spectroscopy of Organic Compounds.* New Delhi: Wiley Eastern; 1985.
23. Boopathi K, Ramasamy P, Bhagavannarayana G. *J Cryst Growth*. 2014; 386: 32–37p.
24. John Coates. Interpretation of Infrared Spectra: A Practical Approach. In: Meyers RA, editor. *Encyclopedia of Analytical Chemistry.* Chichester: John Wiley & Sons Ltd.; 2000; 10815–10837p.
25. Dalhus B, Gorbitz CH. *Acta Chem Scand*. 1996; 50: 544p.
26. Duval C, Mikrochim. *Acta*. 1957; 326p.
27. Socrates G. *IR Characteristic Group Frequencies*. New York: Wiley-Interscience; 1994.
28. Puhal Raj A, Ramachandra Raja C. *Spectrochimica Acta Part A.* 2012; 97: 83–87p.
29. Rajadurai G, Puhal Raj A, Pari S. *Arch Appl Sci Res*. 2013; 5(3): 247–253p.
30. Rajendran KV, Jayaraman D, Jayavel R, *et al. J Cryst Growth*. 2003; 254: 461p.
31. Krishnakumar V, John Xavier R. *Spectrochem Acta A*. 2004; 60: 709p.
32. Li K, Yang P, Xue D. *Acta Mater*. 2012; 60: 35p.
33. Zhao X, Bao Z, Sun C, *et al. J Cryst Growth*. 2009; 311: 711p.
34. Balakrishnan T, Ramamurthy IK. *Mater Lett*. 2008; 62: 65p.
35. Xue D, Zhang S. *J Phys Chem A.* 1997; 101: 5550p.
36. Jeffery GH, Bassett J, Mendham J, *et al. Vogul's Text Book of Quantitative Chemical Analysis*. UK: ELIBS, Addison Wesley Longman Limited; 1989.
37. Priya R, Krishnan S, Raj *et al. J Cryst Res Technol*. 2009; 44: 1272p.
38. Kurtz SK, Perry TT. A Powder Technique for the Evaluation of Nonlinear Optical Materials. *J Appl Phys*. 1968; 39(8): 3798–3813p.
39. Xue DF, Zhang SY. Chemical Bond Analysis of the Correlation between Crystal Structure and Nonlinear Optical Properties of Complex Crystals. *Physica B Condens Matter*. 1999; 262(1–2): 78–83p.
40. Moitra S, Kar T. *Cryst Res Technol*. 2010; 45(1): 70–74p.
41. Wang Y, Eaton DF. *Chem Phys Lett.* 1985; 120: 441p.

Cite this Article

S. Bagavathi, C. Krishnan, P. Selvarajan. The Effect of L-Valine on the Growth and Characterization of Lithium Sulphate Monohydrate Single Crystals. *Research & Reviews: Journal of Physics*. 2019; 8(1): 92–103p.

